RSC Advances

COMMUNICATION

View Article Online
View Journal | View Issue

Cite this: *RSC Adv.*, 2014, **4**, 56848

Facile method to sort graphene quantum dots by size through ammonium sulfate addition†

Seongwoo Ryu,‡[a] Kyueui Lee,‡[a] Soon Hyung Hong[bc] and Haeshin Lee*[ac]

Received 12th July 2014
Accepted 15th October 2014

DOI: 10.1039/c4ra07032a

www.rsc.org/advances

We report a method to purify graphene quantum dots size simply by adding ammonium sulfate. The addition of a salt to a heterogeneous GQD suspension results into the sorting of GQD sub-populations with diameters corresponding to 2.7 ± 1.6, 5.1 ± 1.5, 13.3 ± 1.9, and 18.7 ± 4.4 nm. These GQDs also exhibit different optical properties.

Since the discovery of graphene in 2004,[1,2] it has received much attention because of its extraordinary mechanical, thermal, electrical[3–7] and bio-sensing abilities.[8,9] Because of its metallic property, controlling the bandgap of graphene is a common research goal. It was theoretically predicted that a few nanometers of graphene, known as graphene quantum dots (GQDs), can exhibit bandgap properties similar to those of conventional semiconducting materials.[10] Subsequently, GQDs were experimentally prepared, showing luminescence because of the presence of bandgaps.[11–13] The unique properties of GQDs result into a variety of applications, including photovoltaic devices,[14] organic light-emitting diodes,[15] fuel cells[16] and biological imaging applications.[17,18]

Several methods have been reported for the preparation of GQDs. Nanolithography,[19] hydro/solvothermal cutting,[18,20] electrochemical scissoring,[14] chemical exfoliation,[21] and the decomposition of fullerene[22] can all be used to produce GQDs. These methods can be divided into two categories. The first one includes methods that can prepare homogeneous GQDs of a particular dimension; however, these are not scalable. Nanolithography and the decomposition of fullerene are methods that belong to this category. The second group includes methods that are scalable; however, the dimensions of these GQDs are heterogeneous. Hydro/solvothermal cutting, electrochemical scissoring and chemical exfoliation are examples of these methods. Upon comparing the scalability and the homogeneity of GQDs, it is quite evident that scalability is the more important feature for the aforementioned applications. However, none of the previously developed methods can precisely control the dimensions of GQDs. The use of GQDs with a narrow geometric distribution can greatly improve the performance of GQD-containing devices. Most existing methods are able to produce GQDs with an average diameter of 4–6 nm. In addition, the total synthesis of colloidally stable GQDs has also been reported.[23] The study used oxidative condensation reactions, but it requires repetition of synthesis and multiple purifications to control the size of the synthesized GQDs.

Methods for the preparation of homogeneous inorganic quantum dots of a particular dimension have also been established.[24] Thus, the development of an equivalent method for preparing GQDs with a narrow size distribution is also important. Herein, we report a method that can prepare GQDs with a narrow size distribution, and the distribution is controllable. We were able to effectively collect GQDs with average diameters of 2.7 ± 1.6, 5.1 ± 1.5, 13.3 ± 1.9, and 18.7 ± 4.4 nm ($n = 60$) for the first time without using a column. The ability to control the dimension of GQDs originates from the capability of salts to differentiate among the solubilities of the individual GQDs. We used ammonium sulfate [$(NH_4)_2SO_4$] for GQD purification, which is known as the most effective agent for salting-out proteins, according to the Hofmeister series (lyotropic series).[25]

[Anions]: $SO_4^{2-} \approx F^- > HPO_4^{2-}$ > acetate > $Cl^- > NO_3^- > Br^- > ClO_3^- > I^- > ClO_4^- > SCN^-$

[Cations]: $NH_4^+ > K^+ > Na^+ > Li^+ > Mg^{2+} > Ca^{2+}$ > guanidinium

The reason for choosing the salting-out method, which has been used by biologists for a long time,[25] is the molecular similarity between the GQDs and the mixtures of various proteins. The first reason is the heterogeneity in size. CMG prepared by the modified Hummers method exhibits a size

[a]*Department of Chemistry, Korea Advanced Institute of Science and Technology (KAIST), 291 University Rd., Daejeon 305-701, Republic of Korea. E-mail: haeshin@kaist.ac.kr*

[b]*Department of Materials Science and Engineering, Korea Advanced Institute of Science and Technology (KAIST), 291 University Rd., Daejeon 305-701, Republic of Korea*

[c]*Center for Nature-inspired Technology (CNiT) in KAIST Institute for NanoCentury, Korea Advanced Institute of Science and Technology (KAIST), 291 University Rd., Daejeon 305-701, Republic of Korea*

† Electronic supplementary information (ESI) available. See DOI: 10.1039/c4ra07032a

‡ S. Ryu and K. Lee equally contributed to this work.

heterogeneity, corresponding to the different molecular weights of each protein in the mixture. Furthermore, the molecular weight of GQD is similar to that of the typical water-soluble small proteins. Considering the length of a carbon bond,[26] the estimated molecular weight of the square-shaped, single-layered 10 nm GQD is approximately 30 kDa, without considering the defects or the other functional groups. This value belongs to the molecular weight range (10–60 kDa) of a number of well-known water-soluble proteins such as lysozyme (~14 kDa), green fluorescent proteins (~27 kDa), and albumin (~66 kDa). Moreover, a previous study reported that dialysis, which has been widely used for protein purification, could be a method to separate GQDs,[27] indicating that the dimension of GQDs is similar to that of the water-soluble proteins. The second reason is the presence of charges on the edge of the CMGs or on the surface of proteins. CMG oxidation results in the generation of 'hydrophilic' polar groups, such as hydroxyl and carboxyl groups, along its periphery, which is similar to the presence of polar amino acid residues, such as glutamic acid and aspartic acid (*i.e.* R–COOH), as well as serine and threonine (R–OH). Furthermore, there are hydrophobic, carbon-rich amino acids, for example, isoleucine, valine, phenylalanine, and tryptophan, which is similar to the presence of benzene and other carbon-rich molecules in CMG. Recently, some studies demonstrated that the co-existence of hydrophilic and hydrophobic domains results in conformational changes of CMG similar to protein folding in a salt solution.[28,29] In general, for the case of protein purification, large (*i.e.* high MW) and hydrophobic proteins are salted out first at a low concentration of $(NH_4)_2SO_4$, and then small (*i.e.* low MW) hydrophilic ones are precipitated out later at a high salt concentration. Similarly, we could expect that large, hydrophobic CMGs would be precipitated first, and the small, hydrophilic GQDs would be salted out at a later stage. Because of the predominant existence of hydrophilic groups at the edge of GQDs,[30] the contribution from the hydrophilic edge could become dominant when the GQD size is reduced, thus resulting into an increase in the solubility of the GQDs.

We purified a colloidal GQD sub-population from a heterogeneous chemically modified graphene (CMG) suspension synthesized by a modified Hummers method (first tube, Fig. 1(a)). Fig. 1(a) illustrates the role of ammonium sulfate. Its initial role is the removal of large CMG flakes (>50 nm) simply by the addition of a low concentration of ammonium sulfate (50 mM) (second tube). This concentration of ammonium sulfate effectively causes the immediate aggregation of large flakes of CMG, *i.e.*, graphene oxides. The agglomerated CMGs can easily be removed by centrifugation (10 000 rpm for 5 min) (third tube). After centrifugation, a suspension of very small yet heterogeneous GQDs is obtained (fourth tube). The other role of ammonium sulfate is to sort the sizes of the GQDs by changing the final concentration. The detailed results are given in Fig. 2. Briefly, we found that the sizes of the GQDs decreased as the salt concentration is increased (TEM images, Fig. 1(a)). Each sub-population is collected simply by adding different concentrations of ammonium sulfate. The unwanted, large GQDs can be precipitated by the aforementioned 'salting-out' effect, which is followed by centrifugation. Finally, the supernatant is dialyzed in water.

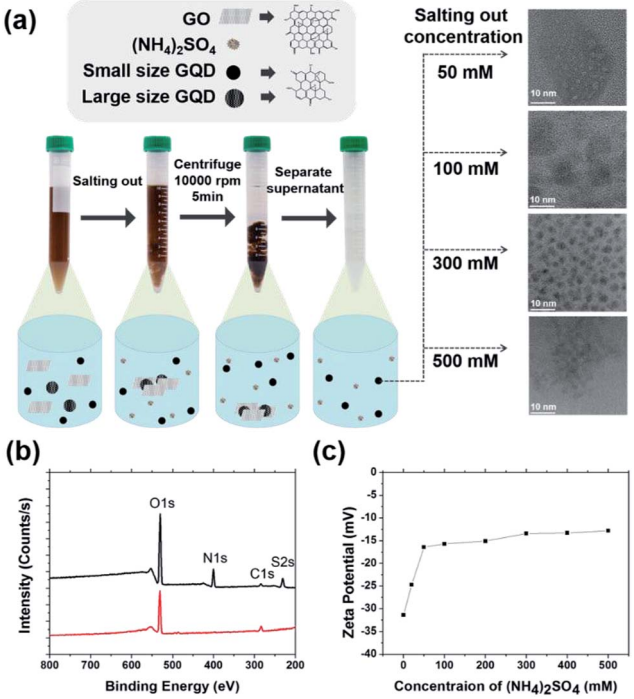

Fig. 1 Schematic of the GQD salting-out procedure: (a) first, the CMG solution was prepared (first tube), after which the salt was added (second tube). Centrifugation was then conducted (third tube), after which the supernatant solution was obtained (fourth tube). As the salt concentration increases, smaller GQDs are purified from the supernatant. (b) XPS spectra of the GQDs before (black) and after dialysis (red) for removing the added salt. After removing the salt, the N 1s and S 2s peaks from the salt were not observed. (c) The zeta potential of GQDs as a function of the salt concentration. The zeta potential value was increased to −16.4 mV (up to 50 mM), after which it did not change throughout the entire salting-out scale.

To examine the degree of ammonium sulfate contamination, we utilized X-ray photoelectron spectroscopy (XPS). Fig. 1(b) shows the GQD flakes before and after dialysis, which was used to determine the presence of ammonium sulfate. Before dialysis, the nitrogen 1s photoelectron (N 1s) peak appeared around 400.0 eV and the sulfur 2p (S 2p) peak appeared at 231.5 eV from the salt, $(NH_4)_2SO_4$ (black). However, the characteristic salt peaks completely disappeared after dialysis (red). This result indicates that the purified GQDs do not contain residual salt ions, which could act as contaminants. The minor degree of interaction between the GQDs and the salt as demonstrated by the XPS results was further demonstrated by the zeta potential (Fig. 1(c)). Each purified GQD sample (GQD50, GQD100, GQD300, and GQD500) showed a similar level of negative charge, ~−15 mV, with a slight tendency of an increased zeta potential from −16.4 mV (GQD50) to −12.8 mV (GQD500). Throughout this study, GQD100 represents the GQDs purified by adding 100 mM of ammonium sulfate. Similarly, the GQDs purified with 500 mM of ammonium sulfate are referred to as GQD500.

The purified GQD sub-populations exhibited differences in their chemical compositions, *i.e.* in their functional groups (Fig. S1†). The high-resolution C 1s spectra showed differences in the carbon chemistries between the GQD50 and GQD100

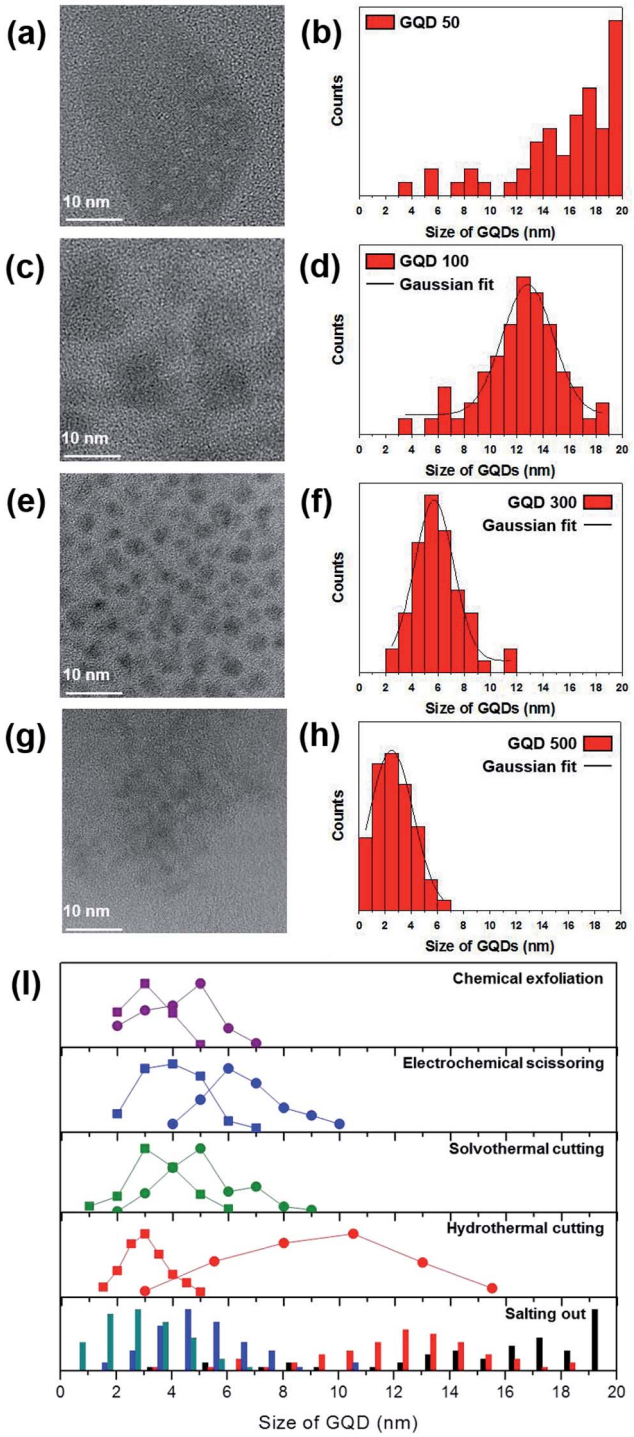

Fig. 2 Size distribution of the purified GQDs: (a) a typical TEM image of GQD50 and its corresponding size distribution (b). (c) A TEM image of GQD100 and its corresponding size distribution (d). (e) A TEM image of GQD300 and its corresponding size distribution (f). (g) A TEM image of GQD500 and its corresponding size distribution (h). ($n = 60$) (i) Overall histograms of the samples purified with the salting-out process: GQD50 (black), GQD100 (red), GQD300 (blue), GQD500 (green) and comparisons with various GQD synthesizing methods.

samples. The major C–C photoelectron peak that appeared at 284.5 eV was more significant in GQD100 (second, red) than that in GQD50 (first, black). The increased C–C photoelectron peak was unchanged for the GQDs purified with higher concentrations of ammonium sulfate (blue for GQD300 and green for GQD500). In general, the large GO or GQD (>20 nm) show higher oxidative levels than the nano-sized GQDs that are smaller than 4 nm. In particular, the oxidation of GQDs primarily appears at the edge with the functional carboxyl or hydroxyl groups (Fig. S1†). The reason for the edge distribution of the functional groups may be the preferential chemical cleavage toward an in-plane oxygen-containing functional group such as an epoxide or a carbonyl group.[20,31] After the cleavage, the oxygen-containing functional group, such as the hydroxyl and carbonyl groups, are located alongside at the edge of the GQDs. Therefore, the charges on the GQDs are found mainly along the periphery (Fig. S2(a)†). Moreover, as the internal core region of GQDs is relatively hydrophobic, and the overall charge density increases when the size of GQDs gets smaller (Fig. S2(b)†).

Raman spectroscopy was also used to characterize the vibrational modes of the GQDs (Fig. S3†). The Raman spectrum of the GQDs after salting-out exhibited a D-band at 1354 cm^{-1} and a broad G-band at 1594 cm^{-1}. The I_D/I_G values were gradually increased from 0.75 for GQD50, 0.78 for GQD100, 0.80 for GQD300, and 0.84 for GQD500. Considering the fact that GQDs were generated by preferential chemical cleavage along the defected, oxygenated areas, we can conclude that the edge GQDs are rich in oxygen-containing moieties and that the inside core is rich in graphitic carbon. Thus, when the size is decreased, the I_G value is expected to decrease because of the increase in the edge perimeter length to core ratio. XRD experiments were also performed, but no significant differences were observed.

The TEM analysis demonstrated that the simple addition of the salt allowed the sorting out of the size of GQDs. Fig. 2 shows TEM images of GQDs purified in the presence of $(NH_4)_2SO_4$ (50, 100, 300, and 500 mM), and the corresponding size distributions are shown in the histograms. Representative TEM images for the sample purified in the presence of 50 mM of $(NH_4)_2SO_4$ (Fig. 2(a) and (b)) exhibit mostly large, chemically modified graphene (CMG) and GQDs between 10 and 20 nm in diameter, with a population distribution of approximately 70%, with the remaining 30% larger than 20 nm in diameter (18.7 nm on an average, with a standard deviation (SD) of 4.4 nm; $n = 60$). With an increase in the salt concentration, we were able to obtain more homogeneous, small GQDs (Fig. 2(c)–(h)). For GQD100, the diameters of the GQDs were 13.3 nm on average with an SD of 1.9 nm ($n = 60$) (Fig. 2(c) and (d)), whereas for GQD300, the average diameter was 5.1 nm with an SD of 1.5 nm ($n = 60$) (Fig. 2(e) and (f)). Finally, for GQD500, the average diameter was 2.7 nm with an SD of 1.6 nm ($n = 60$) (Fig. 2(g) and (h)). Atomic force microscopy (AFM) height profiles confirmed the thicknesses of the purified GQDs (Fig. S4†). Previously, GQDs with a large diameter (>22 nm) showed multiple layers (more than five layers) to some degree.[27] However, multi-layered GQDs were not observed in this case. It has been reported that the height of single-layer graphene can vary from 0.3 to 1.6 nm according to the AFM measurements.[1,32,33] According to the AFM height profiles in this study, most of the GQD particles purified using 500 and 300 mM of $(NH_4)_2SO_4$ showed AFM height profiles of

approximately 0.8 nm, indicating one layer of graphene (Fig. S4(a)–(d)†). Note that the lateral sizes of the purified GQDs were similar across the samples. In general, the tip geometry causes an inaccuracy in the lateral size determination particularly for the small nanoparticles. The relatively large GQD samples of GQD50 and GQD100 showed one to two layers of graphene (Fig. S4(e)–(h)†). The difference in the number of graphene layers can be another advantage of the salting-out method over the existing methods currently being used for preparing GQDs. Fig. 2(i) shows the comparative histograms of the size distributions of GQDs after the proposed salting-out method (bottom) and after chemical exfoliation (purple),[21,34] electrochemical scissoring (blue),[14,35] solvothermal cutting (green),[18,36] and hydrothermal cutting (red).[20,37] In general, most GQD synthesizing methods show either wide-ranging heterogeneous distributions (*e.g.*, hydrothermal cutting) or narrow-range yet uncontrollable size distributions. More specifically, the hydrothermal cutting method led to GQDs of 1 to 16 nm in size, whereas the other methods showed size distributions of less than 10 nm. Importantly, the salting-out method was able to control the size of the GQDs depending on the salt concentration.

The high-resolution TEM (HRTEM) results showed that the edge structures of the purified GQD exhibit both zigzag (red lines in Fig. 3(b) and (c)) as well as armchair (blue lines in Fig. 3(b) and (c)) configurations. Each edge structure is determined by the bandgap energy and thus defines the optical properties. In general, the bandgap energy rapidly decays to zero eV for the zigzag edge, and slowly approaches 0 eV for the armchair edge.[38] As the purified GQDs exhibit both types of edge structures, the optical properties can predominantly be determined by their individual sizes. Because of the quantum confinement effect,[12,39] the energy bandgap of GQDs is approximately related to the inverse proportion of their sizes. Previously, the largest bandgap value of approximately 3 eV was achieved by reducing the size of the GQDs.[20,38] Fig. 3(d) shows the UV-Vis spectrophotometry absorption results of the GQDs. The salting-out GQDs exhibited wide n–π* transition ranging from 290 nm to 332 nm, which corresponds to 3.85 eV (332 nm) and 4.27 eV (290 nm), respectively.

Salts other than $(NH_4)_2SO_4$ (chosen from the Hofmeister series) resulted in salting-out phenomenon, but the degree of salting-out was not as effective as that shown by $(NH_4)_2SO_4$. Experiments using salts, such as ammonium acetate (NH_4OAc), ammonium chloride (NH_4Cl), and ammonium nitrate (NH_4NO_3), demonstrated that $(NH_4)_2SO_4$ showed the best efficiency in the salting-out procedure, ($(NH_4)_2SO_4$ > NH_4OAc > NH_4Cl), which agreed with the Hofmeister series (Fig. S5(a)†). A similar result was obtained after using a series of sodium salts: sodium sulphate (Na_2SO_4), sodium phosphate ($NaHPO_4$), sodium acetate (NaOAc), sodium chloride (NaCl), sodium nitrate ($NaNO_3$), and sodium iodate (NaI). The concentration of all of these salts was fixed to 50 mM. As expected, a fraction of the hydrophobic CMGs in the heterogeneous mixture began to be salted out even by utilizing the sodium-containing salts. However, the efficiency of the salting-out procedure decreased as compared to that of ammonium sulphate: $(NH_4)_2SO_4$ > Na_2SO_4 > $NaHPO_4$ > NaOAc > NaCl > $NaNO_3$ > NaI (Fig. S5(b)†).

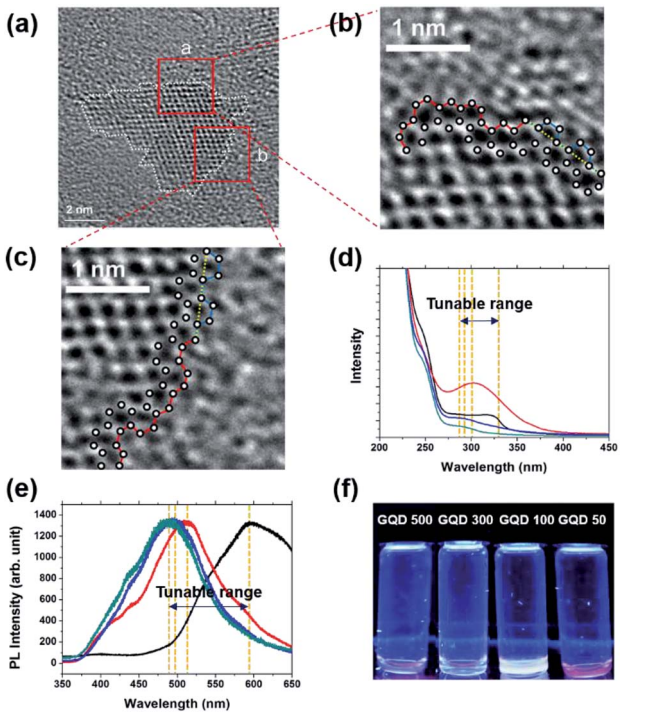

Fig. 3 (a) TEM images of the purified GQDs and magnified images for examining the edge structures. (b) Location 'a' and (c) location 'b'. (b and c) The red lines indicate the zigzag edges of the GQDs, and the blue lines show the armchair edges of the GQDs. (d) UV-Vis absorption results (Abs) of the GQD50 (black), GQD100 (red), GQD300 (blue), and GQD500 (green) supernatants from the CMG suspensions and (e) their corresponding PL spectra (E_{ex} = 325 nm). (f) GQD suspension placed on a 312 nm UV lamp: from the left, GQD500, GQD300, GQD100 and GQD50.

This result showed that any salt in the Hofmeister series generally exhibits dehydration from the macromolecular solutes, thus resulting in salting-out. The characterization of the physicochemical properties of the precipitant and supernatant from each salt could be a topic for further study.

As the sizes of GQDs were reduced (*i.e.*, when they were purified under a high salt condition), the absorption peak was blue-shifted, showing a large amount of bandgap energy.[39–41] This also resulted in large differences in the photoluminescence (PL) emissions (Fig. 3(e) and (f)). The purified GQDs exhibited emissions of 596 nm for GQD50, 515 nm for GQD100, 486 nm for GQD300, and 477 nm for GQD500 when the samples were placed under a 312 nm UV lamp. We also detected absorption at 402 nm and 436 nm for the GQD100, 300, and 500 samples, which can be interpreted as the PL from the remaining oxidative functional groups and the mixed edge structures, as is evident from previous theoretical calculations.[12,39]

Conclusions

We demonstrated for the first time that the simple addition of ammonium sulfate could be a scalable means of purifying GQDs with diameters ranging from 2.7 to 18.7 nm. This method does not require any type of column for purification. Depending on the salt concentration, the sizes of the GQDs can be

controlled with a narrow distribution, exhibiting bandgaps ranging from 3.85 eV to 4.27 eV with spectral emissions ranging from 402 nm 596 nm. The scalable purification method using the salting-out process introduced here will play an important role in providing high-quality GQDs for various applications related to GQDs.

Acknowledgements

The authors acknowledge the financial support from National Research Foundation of South Korea: Mid-career scientist grant (2014002855). This work is also supported in part by Center for Nature-inspired Technology (CNiT) in KAIST Institute for NanoCentury (KINC) and World Premier Materials (WPM) from the Ministry of Industry, Trade, and Natural Resources.

Notes and references

1 K. S. Novoselov, A. K. Geim, S. V. Morozov, D. Jiang, Y. Zhang, S. V. Dubonos, I. V. Grigorieva and A. A. Firsov, *Science*, 2004, **306**, 666.
2 A. K. Geim and K. S. Novoselov, *Nat. Mater.*, 2007, **6**, 183.
3 C. G. Lee, X. D. Wei, J. W. Kysar and J. Hone, *Science*, 2008, **321**, 385.
4 A. A. Balandin, S. Ghosh, W. Bao, I. Calizo, D. Teweldebrhan, F. Miao and C. N. Lau, *Nano Lett.*, 2008, **8**, 902.
5 A. H. Castro Neto, F. Guinea, N. M. R. Peres, K. S. Novoselov and A. K. Geim, *Rev. Mod. Phys.*, 2009, **81**, 109.
6 S. Stankovich, D. A. Dikin, R. D. Piner, K. A. Kohlhaas, A. Kleinhammes, Y. Jia, Y. Wu, S. T. Nguyen and R. S. Ruoff, *Carbon*, 2007, **45**, 1558.
7 T. Schwamb, B. R. Burg, N. C. Schirmer and D. Poulikakos, *Nanotechnology*, 2009, **20**, 405704.
8 S. Alwarappan, A. Erdem, C. Liu and C.-Z. Li, *J. Phys. Chem. C*, 2009, **113**, 8853.
9 S. Alwarappan, C. Liu, A. Kumar and C.-Z. Li, *J. Phys. Chem. C*, 2010, **114**, 12920.
10 P. G. Silvestrov and K. B. Efetov, *Phys. Rev. Lett.*, 2007, **98**, 016802.
11 C. Ö. Girit, J. C. Meyer, R. Erni, M. D. Rossell, C. Kisielowski, L. Yang, C.-H. Park, M. F. Crommie, M. L. Cohen, S. G. Louie and A. Zettl, *Science*, 2009, **323**, 1705.
12 K. A. Ritter and J. W. Lyding, *Nat. Mater.*, 2009, **8**, 235.
13 J. Shen, Y. Zhu, X. Yang and C. Li, *Chem. Commun.*, 2012, **48**, 3686.
14 Y. Li, Y. Hu, Y. Zhao, G. Shi, L. Deng, Y. Hou and L. Qu, *Adv. Mater.*, 2011, **23**, 776.
15 L. Tang, R. Ji, X. Cao, J. Lin, H. Jiang, X. Li, K. S. Teng, C. M. Luk, S. Zeng, J. Hao and S. P. Lau, *ACS Nano*, 2012, **6**, 5102.
16 Y. Li, Y. Zhao, H. Cheng, Y. Hu, G. Shi, L. Dai and L. Qu, *J. Am. Chem. Soc.*, 2012, **134**, 18932.
17 X. Sun, Z. Liu, K. Welsher, J. T. Robinson, A. Goodwin, S. Zaric and H. Dai, *Nano Res.*, 2008, **1**, 20312.
18 S. J. Zhu, J. H. Zhang, C. Y. Qian, S. J. Tang, Y. F. Li, W. J. Yuan, B. Li, L. Tian, F. Liu, R. Hu, H. N. Gao, H. T. Wei, H. Zhang, H. C. Sun and B. Yang, *Chem. Commun.*, 2011, **47**, 6858.
19 L. A. Ponomarenko, F. Schedin, M. I. Katsnelson, R. Yang, E. W. Hill, K. S. Novoselov and A. K. Geim, *Science*, 2008, **320**, 356.
20 D. Pan, J. Zhang, Z. Li and M. Wu, *Adv. Mater.*, 2010, **22**, 734.
21 J. Peng, W. Gao, B. K. Gupta, Z. Liu, R. Romero-Aburto, L. H. Ge, L. Song, L. B. Alemany, X. B. Zhan, G. H. Gao, S. A. Vithayathil, B. A. Kaipparettu, A. A. Marti, T. Hayashi, J.-J. Zhu and P. M. Ajayan, *Nano Lett.*, 2012, **12**, 844.
22 J. Lu, P. S. E. Yeo, C. K. Gan, P. Wu and K. P. Loh, *Nat. Nanotechnol.*, 2011, **6**, 247.
23 X. Yan, X. Cui and L. Li, *J. Am. Chem. Soc.*, 2010, **132**, 5944.
24 B. O. Dabbousi, J. Rodriguez-Viejo, F. V. Mikulec, J. R. Heine, H. Mattoussi, R. Ober, K. F. Jensen and M. G. Bawendi, *J. Phys. Chem. B*, 1997, **101**, 9463.
25 P. K. Grover and R. L. Ryall, *Chem. Rev.*, 2005, **105**, 1.
26 D. R. Lide, *Tetrahedron*, 1962, **17**, 125.
27 S. Kim, S. W. Hwang, M.-K. Kim, D. Y. Shin, D. H. Shin, C. O. Kim, S. B. Yang, J. H. Park, E. Hwang, S.-H. Choi, G. Ko, S. Sim, C. Sone, H. J. Choi, S. Bae and B. H. Hong, *ACS Nano*, 2012, **6**, 8203.
28 R. L. D. Whitby, A. Korobeinyk, V. M. Gun'ko, R. Busquets, A. B. Cundy, K. Lászlo, J. Skubiszewska-Zieba, R. Leboda, E. Tombacz, I. Y. Toth, K. Kovacs and S. V. Mikhalovsky, *Chem. Commun.*, 2011, **47**, 9645.
29 R. L. D. Whitby, V. M. Gun'ko, A. Korobeinyk, R. Busquets, A. B. Cundy, K. Laszlo, J. Skubiszewska-Zieba, R. Leboda, E. Tombacz, I. Y. Toth, K. Kovacs and S. V. Mikhalovsky, *ACS Nano*, 2012, **6**, 3967.
30 Y. Q. Dong, J. W. Shao, C. Q. Chen, H. Li, R. X. Wang, Y. W. Chi, X. M. Lin and G. N. Chen, *Carbon*, 2012, **50**, 4738.
31 J.-L. Li, K. N. Kudin, M. J. McAllister, R. K. Prud'homme, I. A. Aksay and R. Car, *Phys. Rev. Lett.*, 2006, **96**, 176101.
32 A. Gupta, G. Chen, P. Joshi, S. Tadigadapa and P. C. Eklund, *Nano Lett.*, 2006, **6**, 2667.
33 C. Casiraghi, A. Hartschuh, E. Lidorikis, H. Qian, H. Harutyunyan, T. Gokus, K. S. Novoselov and A. C. Ferrari, *Nano Lett.*, 2007, **7**, 2711.
34 L.-L. Li, J. Ji, R. Fei, C.-Z. Wang, Q. Lu, J.-R. Zhang, L.-P. Jiang and J.-J. Zhu, *Adv. Funct. Mater.*, 2012, **22**, 2971.
35 M. Zhang, L. L. Bai, W. H. Shang, W. J. Xie, H. Ma, Y. Y. Fu, D. C. Fang, H. Sun, L. Z. Fan, M. Han, C. M. Liu and S. H. Yang, *J. Mater. Chem.*, 2012, **22**, 7461.
36 S. J. Zhu, J. H. Zhang, X. Liu, B. Li, X. F. Wang, S. J. Tang, Q. N. Meng, Y. F. Li, C. Shi, R. Hu and B. Yang, *RSC Adv.*, 2012, **2**, 2717.
37 D. Y. Pan, L. Guo, J. C. Zhang, C. Xi, Q. Xue, H. Huang, J. H. Li, Z. W. Zhang, W. J. Yu, Z. W. Chen, Z. Li and M. H. Wu, *J. Mater. Chem.*, 2012, **22**, 3314.
38 A. D. Güçlü, P. Potasz and P. Hawrylak, *Phys. Rev. B: Condens. Matter Mater. Phys.*, 2010, **82**, 155445.
39 Z. Z. Zhang and K. Chang, *Phys. Rev. B: Condens. Matter Mater. Phys.*, 2008, **77**, 235411.
40 H. T. Li, X. D. He, Z. H. Kang, H. Huang, Y. Liu, J. L. Liu, S. Y. Lian, C. H. A. Tsang, X. B. Yang and S. T. Lee, *Angew. Chem., Int. Ed.*, 2010, **49**, 4430.
41 R. Q. Zhang, E. Bertran and S.-T. Lee, *Diamond Relat. Mater.*, 1998, **7**, 1663.

